Engineering Structures 325 (2025) 119404

Contents lists available at ScienceDirect

Engineering Structures

journal homepage: www.elsevier.com/locate/engstruct

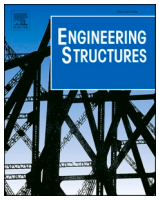

Shear behaviour of deep beams strengthened with high-strength fiber reinforced concrete jackets

Eissa Fathalla [a,*], Boyan Mihaylov [b]

[a] Structural Engineering Department, Cairo University, Giza 12613, Egypt
[b] Urban and Environmental Research Unit (UEE), Univ. of Liège, Building B52, Quartier Polytech 1, Allée de la Découverte 9, B-4000 Liège, Belgium

ARTICLE INFO

Keywords:
Deep beams
Shear
Diagonal cracks
High-strength fiber reinforced concrete (HFRC)
Steel fibers

ABSTRACT

The study addresses the pressing need for effective strengthening of reinforced concrete (RC) members, specifically focusing on shear-critical deep beams. One of the most effective methods for strengthening RC members is the fiber reinforced concrete (FRC) jackets. However, limited number of studies have been conducted on deep beams strengthened with FRC. To address this gap, this paper presents an experimental investigation for strengthening of shear-critical deep beams using high-strength fiber reinforced concrete (HFRC) jackets. The experimental program involves testing three large-scale deep beams, including a reference specimen and two strengthened beams with thin HFRC jackets of different thicknesses (34 mm and 26 mm). The HFRC jackets featured straight steel fibers with a volumetric ratio of 1.13 %. According to the experimental results and analysis, it is found that an HFRC jacket of 34 mm thickness upgraded the strength by around 25 % and enhanced the crack control by reducing crack widths by around 50 % at the same absolute load with respect to the reference specimen. From the measured deformed shapes of the compression zone of the specimens, it is concluded that the main principles of the two-parameter kinematic theory of deep beams remain valid for HFRC-strengthened members, and these principles can be used to establish a complete modelling approach for such members.

1. Introduction

In the recent decades, strengthening and retrofitting of reinforced concrete (RC) members has become a matter of significant importance. Reinforced concrete members deteriorate during their lifetime due to several reasons: negative environmental impacts (i.e., corrosion, carbonation), fatigue damage, overloading, material inadequacies, design/construction errors, etc. Consequently, effective strengthening methods are needed to prolong their service life and secure the safety of users given the limited available resources.

Several strengthening methods have been studied in the literature: external prestressing [1,2], bonded steel plates [3,4], fiber reinforced polymer (FRP) sheets [5,6], concrete jacketing [7], and other. Although these methods can improve the load-bearing capacity of RC members, most of them also have properties that can limit their applicability on-site. FRP sheets have low fire resistance and may have debonding issues resulting in premature failures [8]. In other words, they need careful surface treatments, which is not convenient to perform on-site on a large-scale. In the case of external prestressing tendons and bonded steel plates, they have low corrosion-resistance, especially in harsh environmental conditions with chloride-induced corrosion (i.e., coastal structures, presence of de-icing salts) [9]. On the other hand, concrete jacketing is a popular method for strengthening due to its fire and corrosion resistance [10]. However, one of its main disadvantages is the significant section enlargement, which is not favourable in many cases (e.g., fulfilling architectural requirements). Moreover, the use of normal concrete jacketing increases the permanent loads, which results in increased deformations associated with creep [10]. In terms of durability, RC jackets may have issues due to the restrained shrinkage cracks resulting in lower corrosion-resistance. As a conclusion, it is necessary to find relatively compact/light strengthening solutions that provide substantial load-bearing capacity and enhanced crack control for improved durability. One of such solution can be offered by high-strength fiber reinforced concrete (HFRC) [11]. The added fibers not only improve the mechanical properties of concrete, but also bridge the cracks resulting in an enhanced crack control and thus better durability [12–14]. Furthermore, these materials can be applied via shotcrete methods, which allow for more flexible on-site applications [15].

This paper examines the strengthening of a common element of

* Corresponding author.
E-mail address: mahmoud.fathalla@eng.cu.edu.eg (E. Fathalla).

https://doi.org/10.1016/j.engstruct.2024.119404
Received 29 April 2024; Received in revised form 11 October 2024; Accepted 25 November 2024
Available online 30 November 2024

Nomenclature

a	shear span.
b	beam's width.
h	beam's depth.
d	effective depth.
d_{CLZ}	depth of the critical loading zone (CLZ).
l_{b2}	width of the supporting plates.
f_c'	cylinder compressive strength of normal-strength concrete.
$f_{c,HFRC}$	cylinder compressive strength of high-strength fiber reinforced concrete.
E_c	modulus of elasticity of concrete.
a_g	maximum size of coarse aggregates of normal-strength concrete.
$a_{g,HFRC}$	maximum size of coarse aggregates of high-strength fiber reinforced concrete.
ρ_l	reinforcement ratio of flexural reinforcement.
ρ_v	reinforcement ratio of transverse web reinforcement (stirrups).
f_y	yield strength of steel reinforcement.
f_u	ultimate strength of steel reinforcement.
E_s	modulus of elasticity of steel reinforcement.
ε_y	yield strain of steel reinforcement.
ε_u	rupture strain of steel reinforcement.
l_f	length of steel fibers.
d_f	diameter of steel fibers.
V_f	fibers volumetric ratio.
$f_{u,f}$	fibers tensile strength.
V	shear force.
P	total point load= 2 V.
P_u	total load capacity of beam.
Δ_c	vertical crack displacement associated with the shear distortion of the critical loading zone.
Δ_{cu}	ultimate vertical crack displacement of the critical loading zone.
$\varepsilon_{t,avg}$	average tensile strain along the longitudinal flexural steel reinforcement.
l_t	length of the bottom reinforcement within the cracked part of the shear span.
Δ	mid-span deflection of the beam.
x	horizontal distance measured from mid-span.
CLZ	critical loading zone.
DOF	degree of freedom.
DT	displacement transducer.
DIC	digital image correlation.
NSC	normal-strength concrete.
HSC	high-strength concrete.
FRC	fiber reinforced concrete.
HFRC	high-strength fiber reinforced concrete.
SR	surface roughness.

bridges and buildings, namely deep beams with a focus on shear-critical members. These members have low aspect ratio (shear-span-to-effective-depth ratio a/d<2.0) and transfer large shear forces via direct strut action between loads and supports. Most of the investigations conducted on these members involved strengthening using externally-bonded FRP sheets [16–20]. However, there is limited research conducted on deep beams strengthened with FRC or HFRC jackets. The available tests were conducted on small-scale specimens using FRC with steel or polyvinyl alcohol fibers [21,22]. Runao *et al.* [21] investigated the effect of fiber dosages on upgrading the shear strength of deep beams with and without stirrups. According to their results, FRC jackets were effective in upgrading the shear strength of deep beams with stirrups. However, they were less effective in the case of deep beams without stirrups, which might be attributed to wider cracks that are more difficult to control/-bridge with fibers. Li *et al.* [22] studied the shear behaviour of deep beams strengthened with highly ductile FRC. They investigated different test variables such as a/d ratio, stirrup ratio, and jacket thickness. It was demonstrated that the fibers restrained the development of the shear cracks, and the jackets were effective in upgrading the shear strength, especially for larger a/d ratios. Most importantly, in these tests [21,22] partial debonding was reported between the beams and the jackets due to the interfacial conditions, which may result in limiting their strength and deformation capacity. Generally, creating adequate surface roughness before casting the jackets is crucial to ensure composite action and avoid debonding. Additionally, up to our knowledge, there are no experimental studies conducted on the strengthening of large-scale shear-critical deep beams using FRC or HFRC jackets.

In order to address this gap, an experimental program was conducted for large-scale deep beams strengthened with HFRC concrete jackets, which will be the basis for modelling the behaviour of such members. The experimental program included testing of three large-scale deep beams with shear-span-to-effective-depth ratio a/d less than 2.0. One beam was tested as a reference specimen, while the other two beams were strengthened with HFRC jackets with different thicknesses and straight steel fibers with a volumetric ratio of 1.13 %. The beams were provided with low amount of stirrups in simulation of old structures that do not comply with more stringent modern design codes. The paper reports and discusses the tests with the help of detailed measurements including digital image correlation (DIC). Finally, further analysis is conducted based on the two-parameter kinematic theory of deep beams (2PKT) [23,24] to evaluate the key deformations and the effectiveness of the proposed strengthening method.

2. Experimental program

2.1. Test specimens

The experimental program included monotonic testing of three nominally identical reinforced concrete deep beams up to failure. The beams were cast from normal-strength concrete (NSC). One of the beams (P3) served as a reference specimen, while the other beams were strengthened with HFRC jackets with different thicknesses. Thus, the main testing variable for this experimental program is the jacket thickness (34 mm jacket for P1 and 26 mm for P2).

The cross-sectional dimensions of the reference beam were 250 mm × 800 mm, the shear span a was 1200 mm, the effective depth d was 732 mm, and the shear-span-to-effective-depth ratio a/d was 1.64 – see Fig. 1. The HFRC was obtained by mixing high-strength concrete (HSC) with straight steel fibers. The strengthening jackets were applied to beams P1 and P2 after the creation of surface roughness by removing parts of the concrete via robotized water jetting. This roughness is crucial prior to the application of the jackets in order to prevent delamination during loading and ensure composite action of the two concretes (NSC and HFRC). The procedure of the application of the strengthening jackets will be discussed further in the following sections.

The reinforcement details of the beams are shown in Fig. 1. The specimens were reinforced with bottom longitudinal reinforcement of 8∅20 bars which were placed in two layers spaced at 50 mm centre-to-centre, and top longitudinal reinforcement of 2∅20. The beams were also reinforced with a low amount of vertical web reinforcement (stirrups) of ∅8 @ 300 mm. This reinforcement results in a flexural reinforcement ratio ρ_l of 1.37 % and a stirrup ratio ρ_v of 0.134 %. The clear concrete cover of the reinforcement was 25 mm.

As shown in Fig. 1 (bottom), beam P1 was strengthened with HFRC

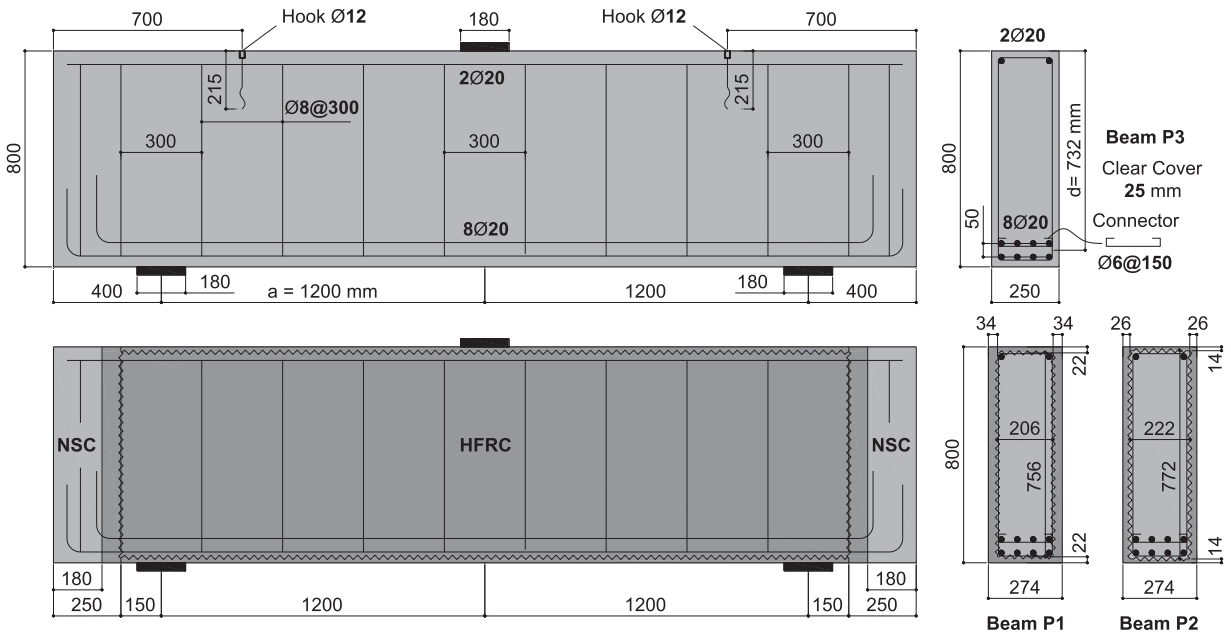

Fig. 1. Geometrical properties and reinforcement details of test specimens.

jacket with an thickness of 34 mm/side and a thickness of 22 mm at each of the top and bottom surfaces (average values). On the other hand, beam P2 was strengthened with a thinner HFRC jacket with a thickness of 26 mm/side and a thickness of 14 mm at each of the top and bottom faces. These strengthening jackets resulted in beams with a total depth h of 800 mm, which is identical to the reference specimen, and a total width b of 274 mm which is higher by ~10 % compared to the reference specimen.

2.2. Material properties

2.2.1. Concrete

The test specimens were cast using NSC, while the strengthening jackets were cast using a commercial product (Groutex Porfil) of HSC [25]. The maximum size of coarse aggregates of NSC and HSC are 22 mm and 2.0 mm, respectively.

For the material characterisation of the hardened concrete in compression, cylinders testing (150 mm × 300 mm) was conducted to obtain the concrete strength f_c. The NSC and HFRC of beams P1 and P2 were cast from the same concrete batch, while the NSC of beam P3 were cast from a different batch. For each concrete batch, a set of three cylinders were cast for testing. In the case of HFRC, two sets of three cylinders were cast: concrete with fibers and concrete without fibers. It should be noted that for each set of cylinders, one cylinder was tested with strain measurements to obtain the modulus of elasticity E_c in addition to the concrete strength, while the other two cylinders were tested to obtain the concrete strength only.

Table 1 summarizes the results from the cylinder tests (average values), in addition to the concrete age at the time of testing. The average compressive strength of the NSC of beams P1 and P2 is 53.0 MPa, while the average compressive strength of beam P3 is 40.5 MPa. On the other hand, the average compressive strength of HSC is 74.0 MPa and 80.7 MPa for HSC without and with fibers, respectively. Generally, the fibers mainly enhance the post-peak resistance of concrete in compression and have a lesser effect on the strength. In this study, the fibers increased the compressive strength of the HSC by ~9 %, which can occur from natural scatter.

Table 1
Material properties of concrete.

Beam	Concrete Type	Compressive Strength	Modulus of Elasticity	Concrete Age
		f_c' (MPa)	E_c (MPa)	(Days)
P1 and P2	NSC	53.0	31,200	559
	HSC (no fibers)	74.0	32,400	201–475
	HSC (with fibers)-HFRC	80.7	30,000	224–551
P3	NSC	40.5	34,300	353

2.2.2. Steel reinforcement

For material characterization of steel in tension, standard tensile testing was performed for one sample of ∅20 and three samples of ∅8 bars. Table 2 summarized the results of tensile testing including yield strength f_y, ultimate strength f_u, modulus of elasticity E_s, and rupture strain ε_u. On average, the bars yielded at ~530 MPa and exhibited a considerable strain hardening behaviour after yielding (f_u/f_y~1.15).

2.2.3. Fibers and tensile behaviour of HFRC

Commercial steel fibers (Dramix OL by BEKAERT) [26] were used for the concrete mix of the HFRC. The steel fibers were straight and smooth with a length l_f of 13 mm and a diameter d_f of 0.2 mm. The nominal tensile strength $f_{u,f}$ is 2750 MPa and the modulus of elasticity is 200 GPa. The fibers volume V_f used in the concrete mix was 1.13 %.

For the characterization of the tensile behaviour of the HFRC, 6 prisms of dimensions 100 mm × 100 mm× 400 mm were tested in symmetrical three-point bending according to the French standard [27] – see Fig. 2. Before testing, a notch with a depth of 6.5 mm and a width of a 2.5 mm was created in the middle section on the bottom side of the prisms via a cutting machine. In the test, a clip gauge for measuring the crack mouth opening was installed in the middle section on the bottom side of the prisms. The tests were performed with a control on the crack opening at a rate of 0.03 mm/min.

Fig. 3 shows the experimental results from the prism tests in terms of

Table 2
Material properties of steel reinforcement.

Bar	f_y (MPa)	f_u (MPa)	E_s (MPa)	ε_u (‰)
∅20	534	616	203,000	97
∅8	523	595	174,000	50

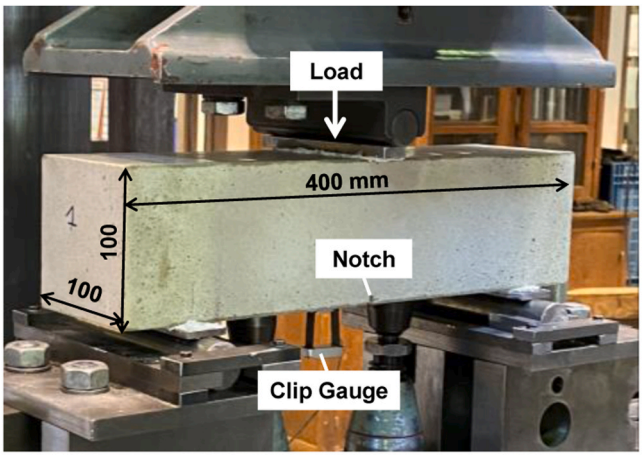

Fig. 2. Three-point bending tests of notched HFRC prisms.

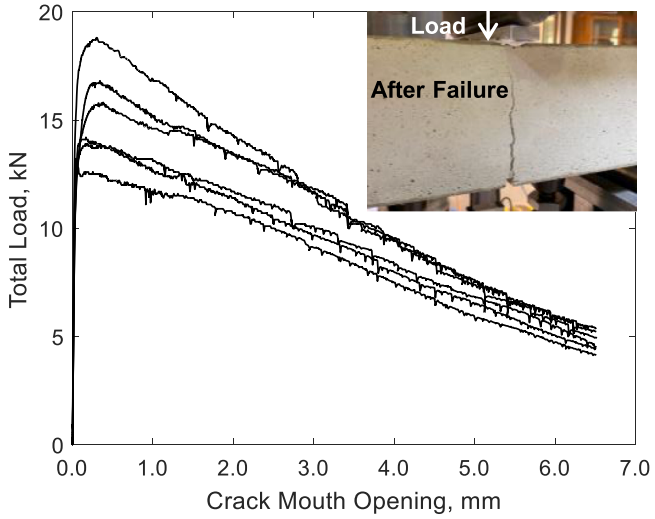

Fig. 3. Experimental results of three-point bending tests on notched HFRC prisms.

load versus crack mouth opening. The prisms failed in flexure in the notched section – see pictogram in Fig. 3. As evident from the results, the flexural strength of the prisms varied between 13.2–18.8 kN. This variation (~40 %) is attributed to the natural scatter in the tensile strength of concrete. On the other hand, in the post-peak response, the scatter was substantially reduced due to the activation of the fibers across the flexural crack, where the response is mainly governed by the fibers.

Finally, using the measurements from the prism tests, an inverse analysis was performed to obtain the relationship between concrete tensile stress and crack opening [27], as shown in Fig. 4. As evident from the results, the HFRC exhibited (on average) a tension-softening behaviour (thick black line) with an average peak resistance of 3.1 MPa.

2.3. Procedure for applying strengthening jackets

Fig. 5 summarizes the steps followed for the application of the strengthening jackets on the hardened concrete beams P1 and P2. The concrete age of the beams at the time of strengthening was 322 days.

Firstly, surface roughness (SR) is created all around the beam section along a central longitudinal distance of ~2700 mm. This roughness is obtained by removing concrete via robotized water jetting – see Fig. 5a. The obtained average SR for beams P1 and P2 was 22 mm and 14 mm, respectively. In the case of beam P1, the rough surface reached the

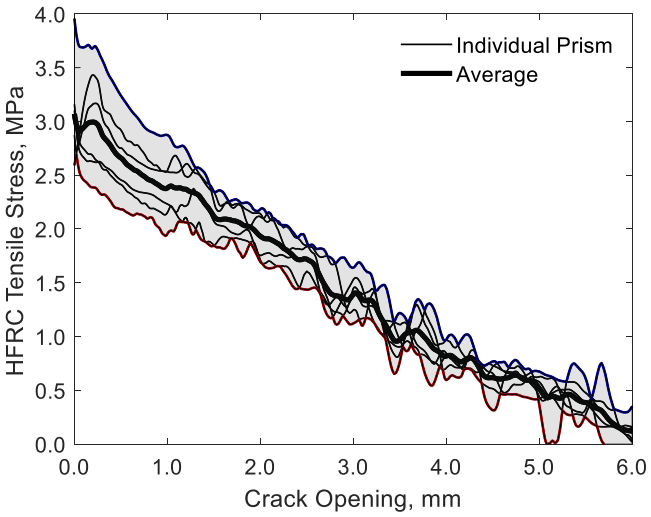

Fig. 4. Tensile response of HFRC obtained from inverse analysis.

stirrups. In the case of beam P2, it was shallower and the stirrups were barely visible – Fig. 5b.

Secondly, formwork was constructed by using plywood on the sides and below the bottom face of the beams. The plywood on the sides of the beams was clamped to the concrete surface via a system of three lateral supporting concrete beams – see Fig. 5d. The sides of the formwork were placed at a distance of 12 mm from the original beam surface in order to ease the flow of HFRC between the formwork and the roughened surface.

Thirdly, the HFRC mixture was prepared by mixing the commercial high-strength cementitious material, water, and steel fibers – see Fig. 5c. Next, the fresh mixture was cast from the top of the formworks. After the casting, a curing compound was added on the top surface of the concrete to maintain the moisture for the hydration process – see Fig. 5e. Finally, the top surface was covered by plastic sheets and the formworks were kept for around 7 days.

2.4. Test setup and instrumentation

Fig. 6 shows the test setup of the deep beam specimens. The beams were tested in symmetrical three-point bending with a shear span a of 1200 mm, which results in a shear-span-to-effective-depth ratio a/d of 1.64. The load was applied via a hydraulic jack with capacity of 2500 kN, which was equipped with a load cell and a spherical hinge. The supports were rollers to allow for unrestrained elongation of the beams during loading. The jack load was transferred to the beams via a loading plate of dimensions 180 mm × 250 mm× 30 mm. The same plate dimensions were used for the supports. A thin layer of plaster was applied between the plates and the concrete surface to ensure full contact.

The same figure also illustrates the instrumentation used for the measurements. Nine displacement transducers were used to capture local and global deformations. They were placed on one side of the beams in a symmetrical manner in the two shear spans. Transducers DT-A and DT-B were used to measure the average elongation along the flexural tensile reinforcement, and DT-C was used to measure the mid-span deflection with respect to a horizontal rod connecting at two supports. DT-D and DT-I were used to measure the vertical crack displacement at a distance of $0.7a$ measured from mid-span, DT-E and DT-H were used to measure the vertical crack displacement at a distance of $0.47a$ from mid-span, and DT-F and DT-G were used to measure the vertical crack displacement at a distance of $0.25a$. It should be noted that the latter 6 transducers were placed along the paths of the expected critical shear cracks.

Moreover, on the opposite side of the beams, three-dimensional

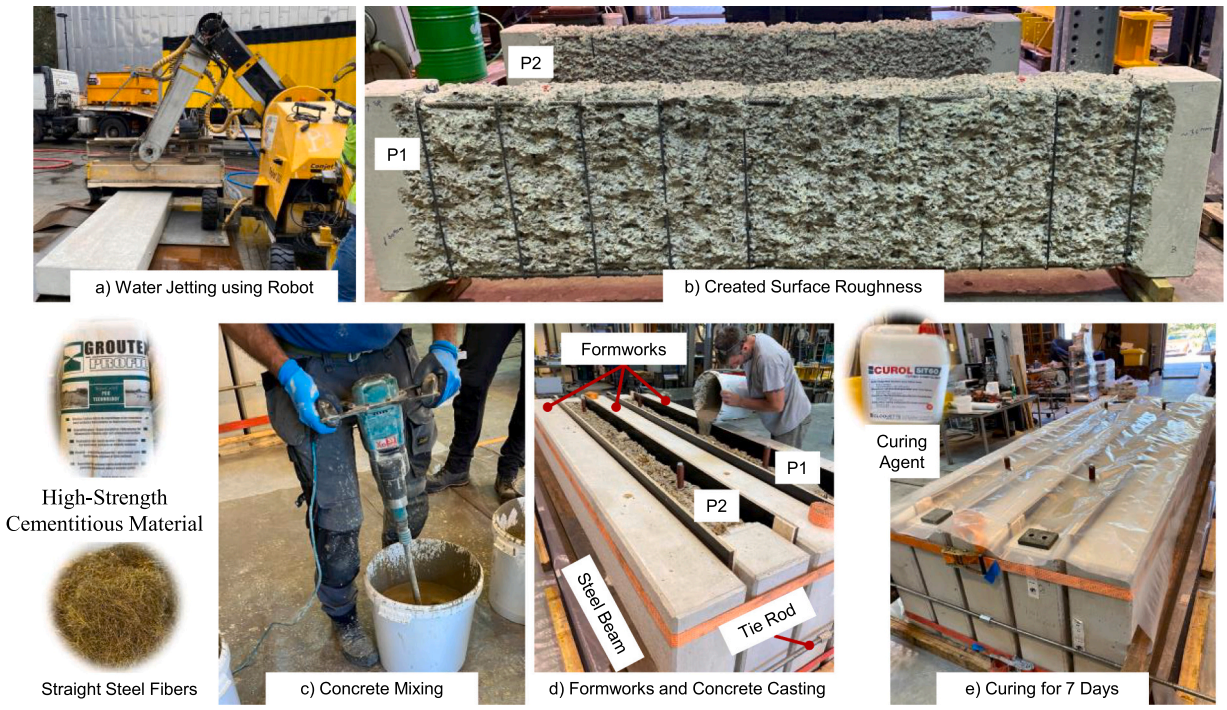

Fig. 5. Procedure for the application of the strengthening jackets to beams P1 and P2.

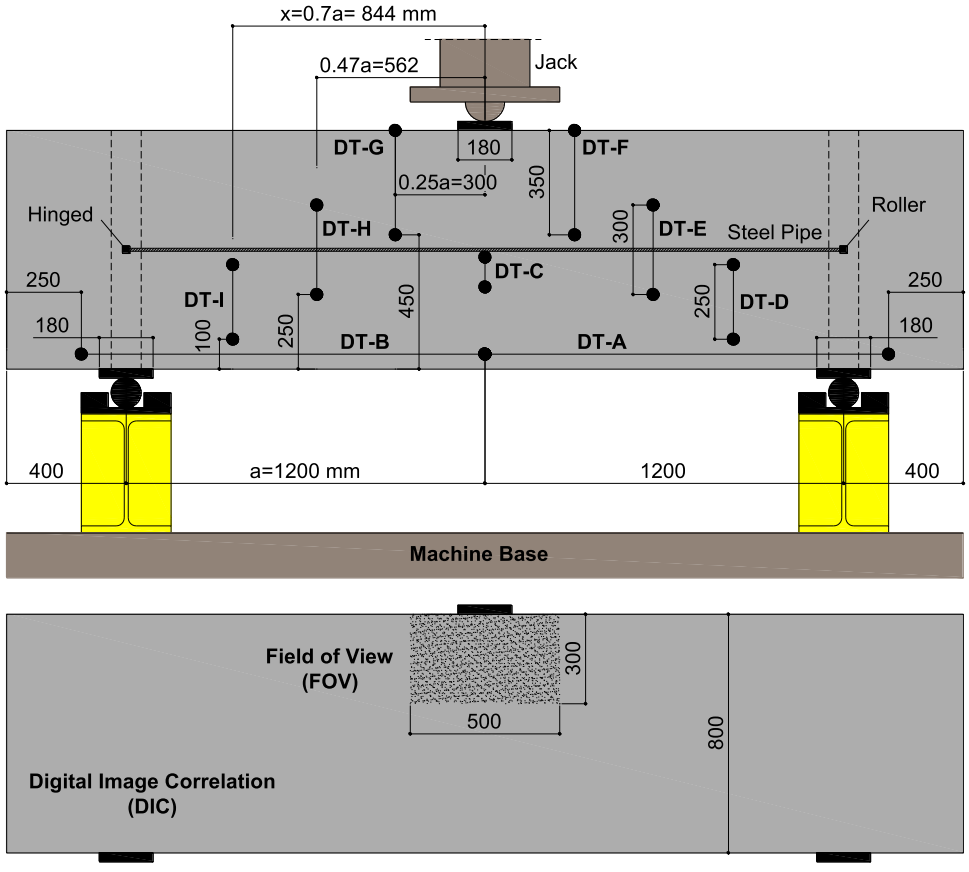

Fig. 6. Test setup and instrumentation of test specimens: front and back beam faces.

digital image correlation (DIC) was performed on the central zone just below the loading plate. The DIC was equipped with two high resolution cameras of 24 mega-pixels to conduct the raw measurements (photos). Before each test, intrinsic and extrinsic calibrations were conducted for the cameras using a relevant calibration board. Next, the calibration score was obtained from software VIC-3D (version 9) [28], and it was in

the order of 0.02–0.03 in demonstration of successful calibration [28]. Subsequently, the raw measurements were conducted, then they were post-processed using the same software. After the analysis, the projection error of each pair of DIC images was checked to ensure that it was within the allowable ranges [28]. At the end, the DIC is capable to capture the deformed shape of this zone, crack displacements, and the concrete strains. To further validate the results of DIC, manual crack width measurements were compared to the corresponding DIC ones and

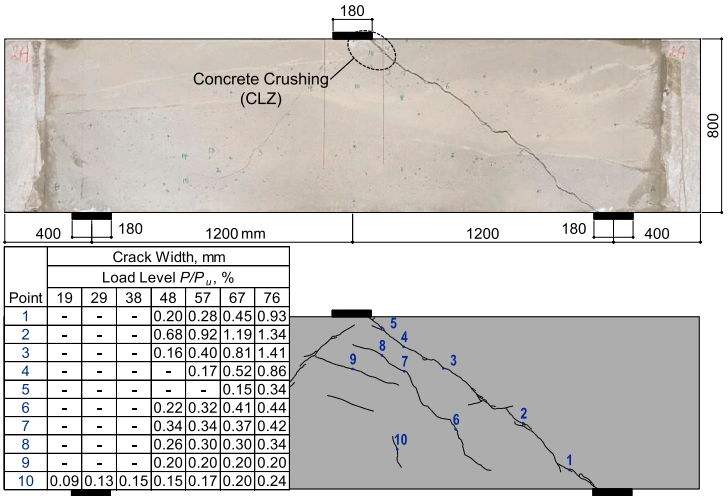

Point	Crack Width, mm Load Level P/P_u, %						
	19	29	38	48	57	67	76
1	-	-	-	0.20	0.28	0.45	0.93
2	-	-	-	0.68	0.92	1.19	1.34
3	-	-	-	0.16	0.40	0.81	1.41
4	-	-	-	-	0.17	0.52	0.86
5	-	-	-	-	-	0.15	0.34
6	-	-	-	0.22	0.32	0.41	0.44
7	-	-	-	0.34	0.34	0.37	0.42
8	-	-	-	0.26	0.30	0.30	0.34
9	-	-	-	0.20	0.20	0.20	0.20
10	0.09	0.13	0.15	0.15	0.17	0.20	0.24

(a) Beam P1: strengthened with HFRC jacket of thickness 34 mm.

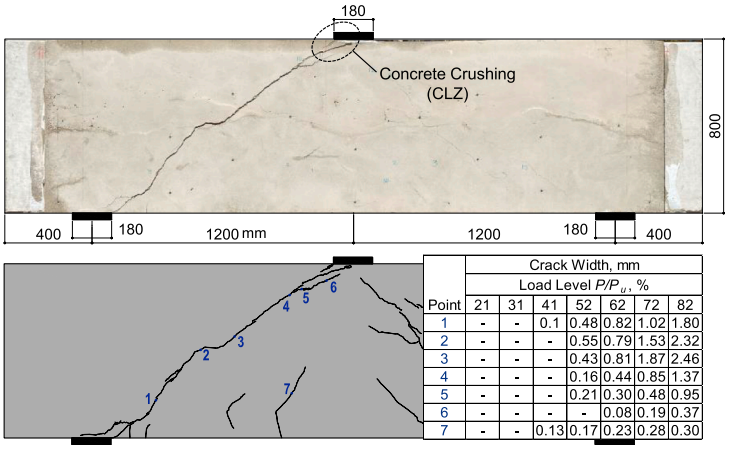

Point	Crack Width, mm Load Level P/P_u, %						
	21	31	41	52	62	72	82
1	-	-	0.1	0.48	0.82	1.02	1.80
2	-	-	-	0.55	0.79	1.53	2.32
3	-	-	-	0.43	0.81	1.87	2.46
4	-	-	-	0.16	0.44	0.85	1.37
5	-	-	-	0.21	0.30	0.48	0.95
6	-	-	-	-	0.08	0.19	0.37
7	-	-	0.13	0.17	0.23	0.28	0.30

(b) Beam P2: strengthened with HFRC jacket of thickness 26 mm.

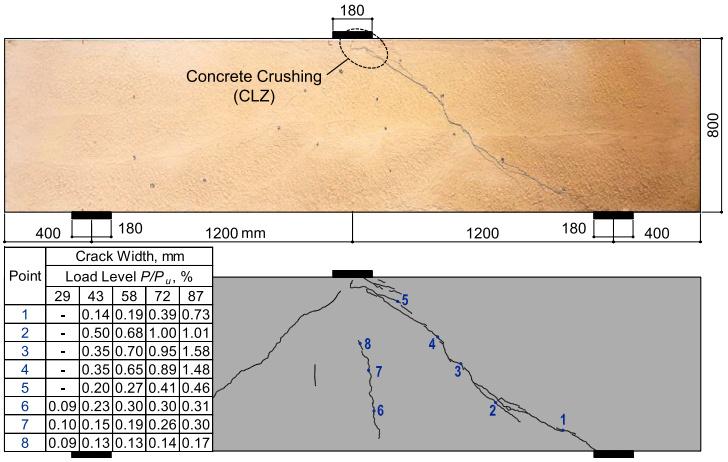

Point	Crack Width, mm Load Level P/P_u, %				
	29	43	58	72	87
1	-	0.14	0.19	0.39	0.73
2	-	0.50	0.68	1.00	1.01
3	-	0.35	0.70	0.95	1.58
4	-	0.35	0.65	0.89	1.48
5	-	0.20	0.27	0.41	0.46
6	0.09	0.23	0.30	0.30	0.31
7	0.10	0.15	0.19	0.26	0.30
8	0.09	0.13	0.13	0.14	0.17

(c) Beam P3: reference specimen.

Fig. 7. Crack patterns of test specimen at failure: photographs (top) and reproduced crack patterns at failure with manual crack width measurements at various load levels (bottom).

they showed good agreement.

2.5. Loading procedure

The beams were tested under monotonic loading in several loading steps of 150 kN, except for the first loading step which reached 300 kN. After each loading step, the load was reduced by 10 % and kept constant to preform crack width measurements and take photos for reporting. The loading was initially performed in a load control (~2 kN/sec) up to the loading step prior to failure. Finally, at the last loading step, the control of the machine was switched to displacement (0.01 mm/sec) in order to capture the post-peak behaviour of the beams.

3. Experimental results

3.1. Global response

The reference beam and the strengthened beams failed in shear by the opening of a critical diagonal shear crack and the crushing of the compression zone near the loading plate (the critical loading zone, CLZ), as shown in Fig. 7. Beam P3 (reference) failed at a total load of 932 kN, while beams P1 (strengthened with HFRC of 34 mm/side) and P2 (strengthened with HFRC of 26 mm/side) failed at a total load of 1417 kN and 1311 kN, respectively. One of the main reasons for the enhancement in strength due to the HFRC jackets is the fibers contribution to the total shear carried by the beams. The fibers were activated by the critical shear cracks and transferred substantial tension across the cracks due to the good anchorage in the HFRC matrix (see Fig. 8 for a close-up photo at one of the locations along critical shear crack).

As evident from Fig. 9, the global behaviour of the three beams was similar in shape. The beams behaved linearly up to ~20 % of their peak resistance P_u when flexure cracks started to occur. Subsequently, a reduction in the tangent stiffness was observed and the beams behaved almost linearly up to ~45 % of P_u, accompanied by the opening of the flexural cracks. After this point, the shear cracks were observed propagating from the supporting plates towards the loading point. It should be noted that the critical shear cracks were stabilized and fully propagated at ~70 % of P_u, reaching the vicinity of the CLZ under the loading plate. With subsequent loading, the beams exhibited slight softening accompanied by the widening of the shear cracks up to ~90 % of P_u. Finally, following this point, a significant reduction in the tangent stiffness of the beams occurred until failure.

Also, Fig. 7 (see reproduced crack patterns) shows the progress of the widths of the measured flexural and shear cracks within the critical shear span. The maximum width of the critical shear crack was observed around the mid-depth of the beams. In terms of crack control at the same absolute load of 700 kN, the maximum crack width of the reference specimen (75 % of P_u) was ~1.1 mm. On the other hand, for the strengthened beams at the same absolute load (49 % of P_u for P1 and

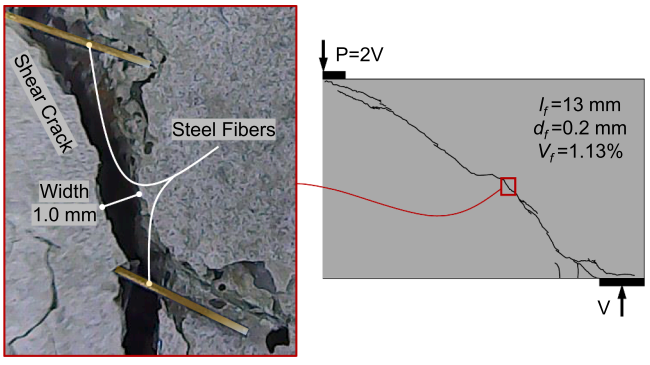

Fig. 8. Close-up photo along critical shear crack showing fibers bridging the crack.

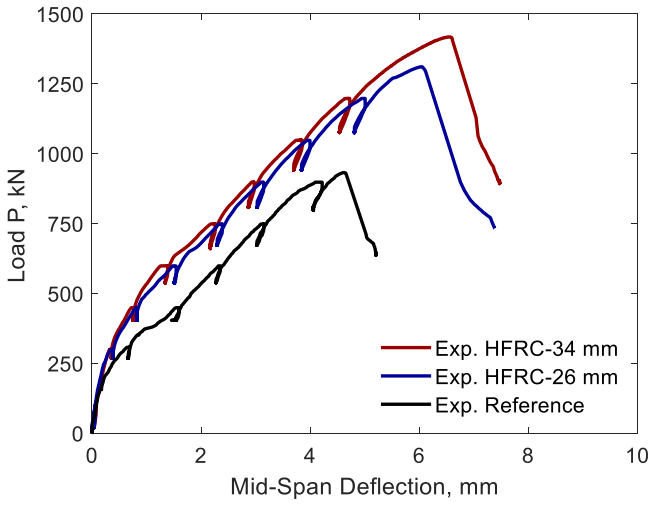

Fig. 9. Global response of the test specimens.

53 % of P_u for P2), the maximum crack width was ~0.6 mm, thus reduced by ~45 %.

Moreover, by comparing the failure crack patterns for the strengthened beams, beam P1 was dominated by two shear cracks within the critical shear span, while P2 was dominated by only one shear crack similar to the reference beam. Therefore, as it can be expected, a thicker HFRC jacket provides better crack control.

Finally, regarding the flexural response, Fig. 10 shows the average strain $\varepsilon_{t,avg}$ along the flexural tensile reinforcement obtained from transducers DT-A and DT-B within the critical shear span. It is clear that the longitudinal flexural reinforcement was in the elastic range ($\varepsilon_{t,avg} < \varepsilon_y$=2.63 ‰) throughout the response reaching maximum values of 2.0 ‰, 1.8 ‰, and 1.35 ‰ at the peak resistance for beams P1, P2, and P3, respectively. It can also be seen that the HFRC jackets stiffened the flexural reinforcement.

3.2. Local deformations

The local deformations along the critical shear crack are discussed in terms of the measured vertical crack displacements. Fig. 11 shows the progress of vertical crack displacements with the increase in load. As evident from the results, the strengthening jackets led to a substantial delay in the formations of the shear cracks. The formation of the critical shear crack for the refence specimen was at ~380 kN, while for the

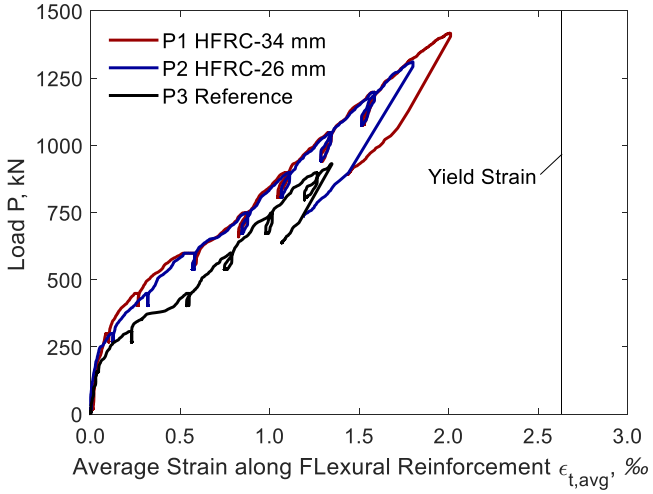

Fig. 10. Flexural response of the test specimens.

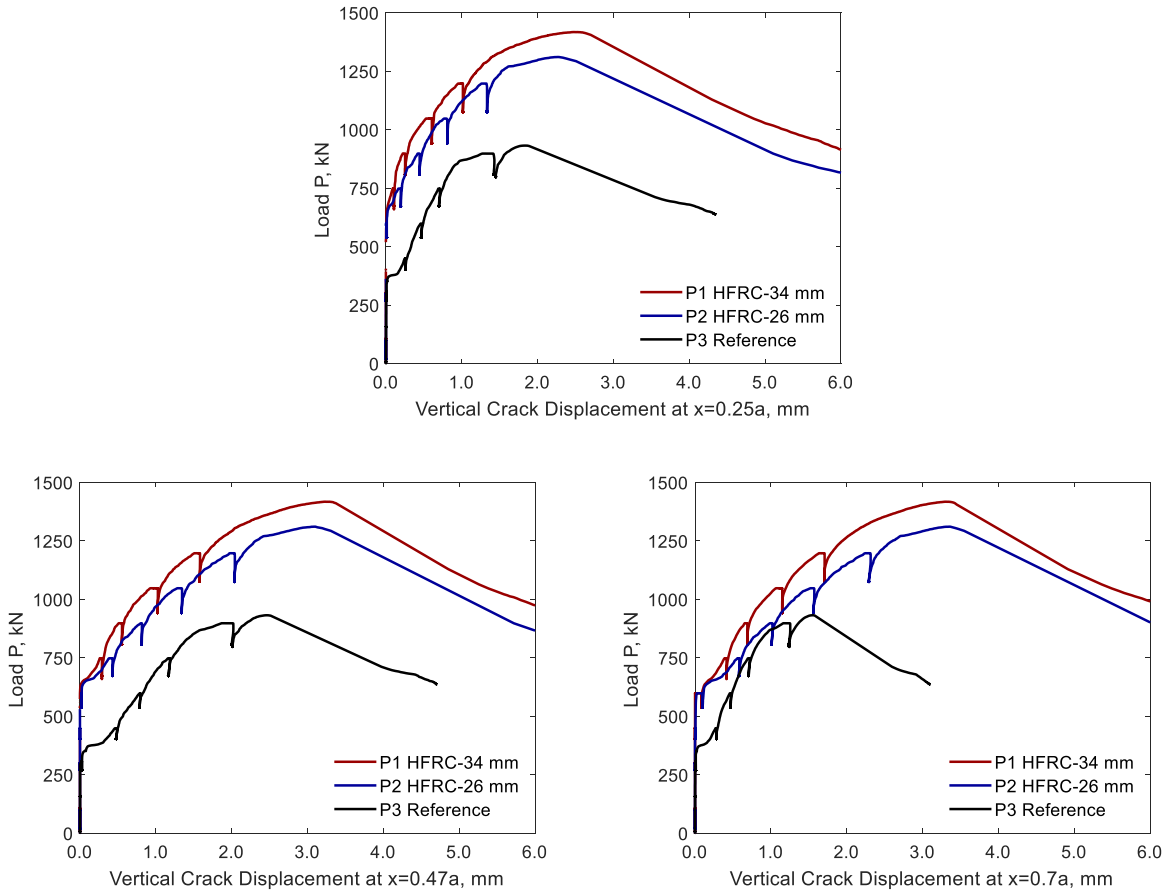

Fig. 11. Vertical crack displacements of the test specimens along the critical shear crack: x is the horizontal distance measured from mid-span and a is the shear span.

strengthened beams it was at ~660 kN with a difference of ~74 %.

Additionally, it is demonstrated again that substantial crack control was provided by the HFRC jackets compared to the reference specimen. For example, at a load of 800 kN, the maximum vertical crack displacement of the reference specimen (P3) was ~1.3 mm. By applying the strengthening jackets, this crack displacement was reduced on average by ~70 % reaching a value of ~0.4 mm in the strengthened beams.

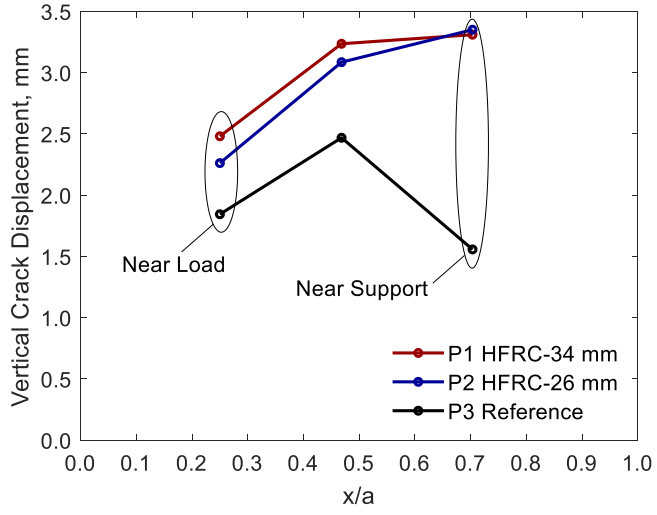

Fig. 12. Distribution of the vertical crack displacements along the critical shear cracks at failure: x is the horizontal distance measured from mid-span and a is the shear span.

In terms of the distribution of the crack displacements along the critical shear crack, Fig. 12 shows the results at failure obtained from the three vertical transducers within the critical shear span. The vertical cack displacement was maximum at around the mid-depth for the reference specimen reaching a value of 2.5 mm. However, for the strengthened beams, the maximum displacement occurred in the bottom half of the beams near the supports. The strengthened beams reached a nearly equal maximum crack displacement of ~3.3 mm. On the other hand, the vertical cack displacements were minimum near the loading plate for all the beams, reaching values of 2.5 mm, 2.3 mm, and 1.8 mm for beams P1, P2, and P3, respectively.

Noticeably, there is a clear reduction in the crack displacements near the support in the case of the reference beam (P3) due to the crack control provided by the tensile flexural reinforcement. However, this crack control is less pronounced for the case of the strengthened beams. The flexural reinforcement in the case of the strengthened beams had a larger concrete cover, and this led to a reduction in the effectiveness of the reinforcement to control the shear crack.

3.3. *Deformed shapes*

The measurements conducted by DIC across the loading zone of the specimens allowed to obtain the deformed shapes of this zone, as shown in Fig. 13. It is immediately evident that the deformed shapes at failure of the reference beam and the strengthened beams had a nearly identical pattern. They all show a rotation of the concrete block above the critical crack around the tip of the crack, as well as a vertical translation of the block. The shear deformations and cracks above the failure crack outline the critical loading zone (CLZ), where concrete crushing was observed.

These measured deformed shapes are well expressed by the two-parameter kinematic theory (2PKT) for deep beams [23]. This

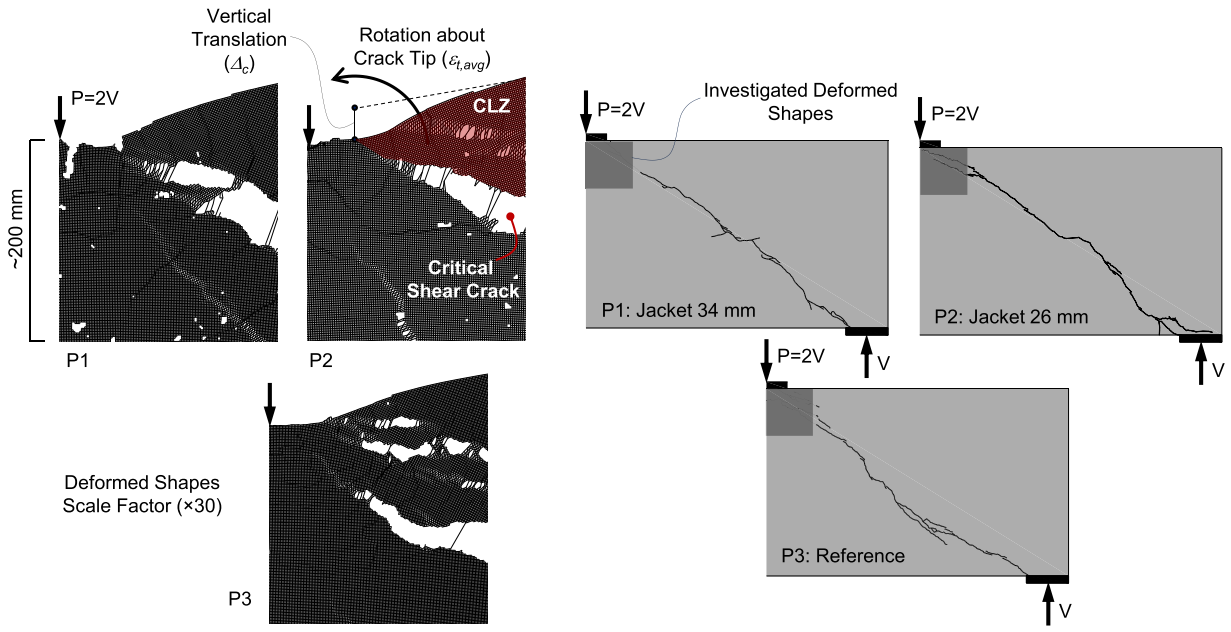

Fig. 13. Measured (DIC) deformed shapes of the compression zone (CLZ) within the critical shear span.

modelling approach assumes that the critical shear crack divides the shear span into two regions: a rigid block above the crack and a bottom region characterized by a series of flexural-shear cracks – see Fig. 14. In the 2PKT, the behaviour of shear-critical deep beams is expressed in terms of two degrees of freedom (DOFs): the average strain of the flexural reinforcement, $\varepsilon_{t,avg}$, and the shear distortion of the CLZ, Δ_c. According to the 2PKT, the rotation of the concrete block above the crack is proportional to DOF $\varepsilon_{t,avg}$. On the other hand, the shear distortion Δ_c is approximately equal to the vertical translation marked in Fig. 13.

4. Kinematic analysis

In the previous section, it was demonstrated that the 2PKT is consistent with the observed deformations in the CLZ. Hence, in this section, the 2PKT [24] is used for further analysis of key deformations and the effectiveness of HFRC jackets.

4.1. DOFs $\varepsilon_{t,avg}$ and Δ_c

The instrumentation of specimens P1-P3 was planned in part to measure the two DOFs of the kinematic model. The average strain of the flexural reinforcement $\varepsilon_{t,avg}$ was measured directly by displacement transducers DT-A and DT-B– see Fig. 10. On the other hand, DOF Δ_c corresponds to the shear distortion of the CLZ. This zone exhibits shortening under diagonal compression – see Fig. 14, where the vertical component of this shortening corresponds to DOF Δ_c. Here, Δ_c can be estimated from the vertical crack displacements within the CLZ, using the DIC measurements. As shown in Fig. 14, both DOFs Δ_c and $\varepsilon_{t,avg}$ contribute to the vertical crack displacements. However, the contribution of DOF $\varepsilon_{t,avg}$ is rather negligible at the top near the loading point. In other words, the vertical crack displacement at the top of the beam is mainly governed by DOF Δ_c. On this basis, DOF Δ_c can be reasonably estimated as the vertical crack displacement at the end of the CLZ along the shear crack (Fig. 14).

To rationally evaluate the end point of the CLZ, a procedure proposed by Trandafir et al. [29] is adopted in this study. In this procedure, a key parameter defining the geometry of the CLZ is the depth of the CLZ, denoted as d_{CLZ}, which is the shortest distance measured from the

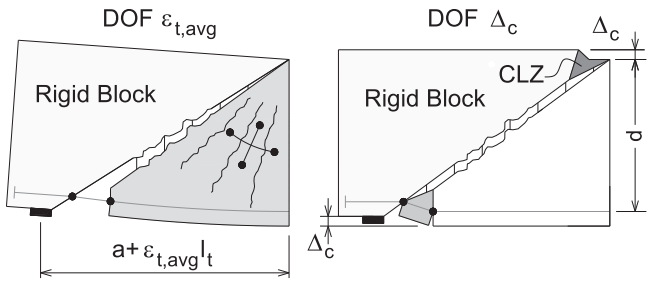

Fig. 14. DOFs of the 2PKT approach for shear-critical deep beams.

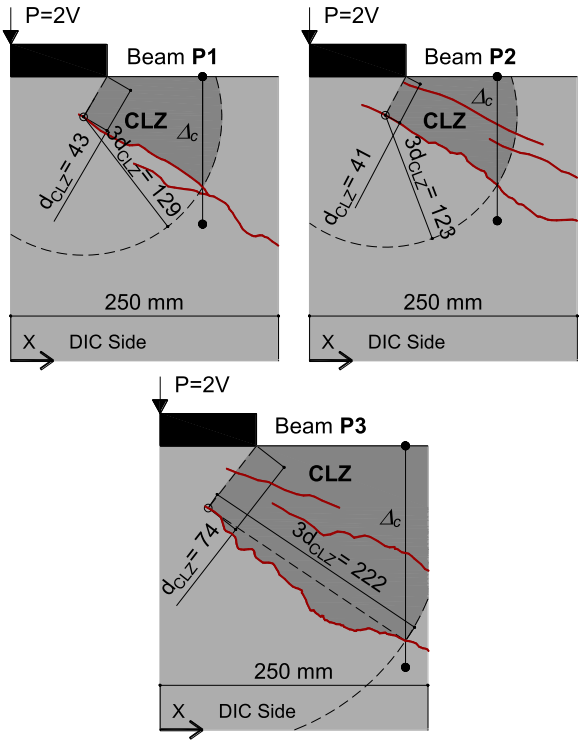

Fig. 15. Estimated locations of vertical crack displacement that correspond to Δ_c.

edge of the loading plate to the critical shear crack. As shown in Fig. 15, the end of the CLZ is estimated as the point at a distance of $3d_{CLZ}$ along the shear crack, measured from the bottom point of d_{CLZ}. It is at this location where DOF Δ_c is measured with a virtual vertical gauge using the DIC results. The gauge crosses the critical crack and all cracks within the CLZ to capture the complete shear distortion of the CLZ. As evident from Fig. 15, cracks in the CLZ were mostly formed in the reference specimen, followed by beam P2 with the thinner jacket. In contrast, for beam P1 with the thicker jacket, no CLZ cracks were formed at failure due to the crack control provided by the jacket with fibers.

Fig. 16 shows the estimated Δ_c including (thick lines) and excluding (thin lines) the cracks within the CLZ. By comparing the thin and the thick lines, it is evident that the secondary cracks began to occur at ~97 % of P_u (just before failure), and they were associated with the beginning of crushing of this zone. In other words, the secondary cracks only contribute to the ultimate value of Δ_c.

Moreover, as evident from the results in Fig. 16, the shear crack propagated rapidly within the CLZ for the reference specimen – note the horizonal portion of the response. However, for the strengthened beams, the propagation of the shear crack occurred in a more gradual manner due to the crack control provided by the fibers. In terms of ultimate deformation, the peak vertical displacements of the CLZ, Δ_{cu}, was nearly the same for the strengthened beams P1 and P2 (1.4 mm), and slightly larger for the reference beam P3 (1.6 mm). This is consistent with the 2PKT, which links Δ_{cu} to a crushing strain of the concrete of 3–3.5 ‰, independent of the concrete strength and fiber content [23].

Table 3 summarizes the measured DOFs at failure, in addition to their contribution to the total deflection of the beams. The deflection is derived from the kinematic model in Fig. 14:

$$\Delta = \Delta_c + \left(\frac{\varepsilon_{t,avg} l_t}{d}\right) a \quad (1)$$

where l_t is the length of the bottom reinforcement within the cracked part of the shear span estimated as $l_t = (a\text{-}l_{b2}/2)/(d/h) = 1016$ mm, a is the shear span (1200 mm), l_{b2} is the width of the support plate (180 mm), h is the total depth (800 mm), and d is the effective depth (732 mm) of the beam.

As evident from the results, DOF $\varepsilon_{t,avg}$ dominated the total deflection by ~65 % compared to DOF Δ_c. Also, it is observed that introducing HFRC jackets increases the contribution of $\varepsilon_{t,avg}$ and reduces the contribution of Δ_c. This is attributed to the fact that the elongation of the flexural reinforcement ($\varepsilon_{t,avg}$) is approximately proportional to the applied load. Finally, by comparing the 2PKT estimated deflection and the measured ones, it can be seen that the 2PKT captures reasonably well the beams global ultimate response with only two DOFs.

Table 3
Measured DOFs and estimated deflection (2PKT).

DOF	P1	P2	P3
Δ_c (mm)	1.4	1.4	1.6
	29 %Δ_{2PKT}	31 %Δ_{2PKT}	42 %Δ_{2PKT}
$\varepsilon_{t,avg}$ (‰)	2.0	1.8	1.4
	71 %Δ_{2PKT}	69 %Δ_{2PKT}	58 %Δ_{2PKT}
Δ_{2PKT} (mm)	4.7	4.4	3.8
$\Delta_{exp.}$(mm)	6.5	6.0	4.6

4.2. 2PKT predictions for the reference specimen

In the previous sub-section, the DOFs of the 2PKT model were evaluated from the experimental measurements. Thus, it is further of interest to compare these measured DOFs with the predicted ones in the case of the reference specimen P3. According to the 2PKT [24], the predicted strength is 1023 kN (vs. measured of 932 kN) with an experimental-to-predicted ratio of 0.91. In terms of local deformations, the predicted DOFs Δ_c and $\varepsilon_{t,avg}$ are 1.15 mm (vs. measured of 1.6 mm) and 1.6 ‰ (vs. measured of 1.4 ‰), respectively. These results show the adequacy of the 2PKT, which has been extensively validated elsewhere [23,24].

4.3. Effectiveness of HFRC jackets based on 2PKT

Based on the experimental measurements, it was shown that HFRC jackets provide substantial crack control, which is beneficial from a durability point of view. Additionally, it was demonstrated that HFRC jackets delay the occurrence of the shear cracks.

In terms of strength, the experimental results show that introducing HFRC jackets with thicknesses of 34 mm and 26 mm led to an increase in the strength by 52 % and 41 %. However, the concrete compressive strength for the reference specimen P3 and the strengthened beams was not the same with a difference of 30 % (f_c=40.5 MPa vs. 53 MPa, respectively). Therefore, the increase in the strength is not only due to the HFRC jackets, but also due to the increase in the compressive strength of the NSC of the beams. In order to tackle this issue, the 2PKT model is used to predict the strength of the reference specimen P3, but with a compressive strength equal to that of the strengthened beams (f_c=53 MPa). According to the 2PKT [24], the predicted strength of P3 * is 1135 kN. In this way, the true effectiveness of the HFRC jackets in terms of the strength can be estimated – see Fig. 17. The results show that the estimated increase in strength for thicknesses of 34 mm and

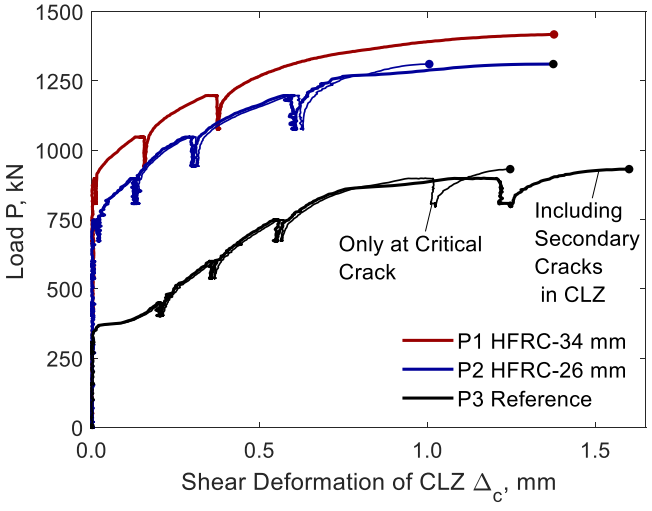

Fig. 16. Measured shear deformation Δ_c of CLZ.

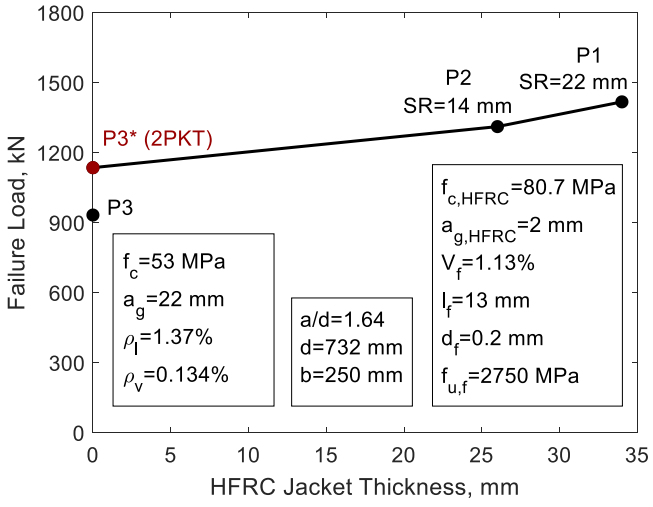

Fig. 17. Effect of HFRC jacket thickness on deep beam's shear strength.

26 mm is 25 % and 16 %, respectively.

5. Conclusions

This paper presented an experimental program of three large-scale shear-critical RC deep beams strengthened with HFRC jackets. The specimens had a total depth of 800 mm and featured low amounts of stirrups (ρ_v=0.134 %). The beams were tested in three-point bending with a shear-span-to-effective-depth ratio a/d of 1.64. The HFRC jackets had straight steel fibers with a volumetric ratio of 1.13 % and variable thickness. Through detailed experimental measurements and kinematic-based analysis, the following conclusions can be drawn:

- Applying relatively thin HFRC jackets (34 mm for beam P1 and 26 mm for P2 on a 250 mm-wide section) provides a substantial control of the shear cracks compared to the reference specimen. This effect was more pronounced for the thicker jacket.
- The application of HFRC jackets results in a significant delay in the initiation of shear cracks compared to the reference specimen, with an approximate increase of 74 % in the initiation load. Consequently, this delay contributes to enhanced durability under service conditions.
- The shear strength of deep beams was upgraded by up to 25 % due to the HFRC jackets. This increase is attributed mainly to the tension in the fibers bridging the critical shear cracks.
- The two-parameter kinematic theory of deep beams (2PKT) describes well the strengthened specimens in terms of deformed shapes and overall behaviour. Therefore, the original 2PKT approach can be extended to predict the shear strength of deep beams strengthened with HFRC jackets.
- While this experimental program focused on studying the effect of jacket thickness on two large-scale deep beam specimens, further investigations are needed to study other variables, e.g. fiber volume and mixes with strain-hardening properties.

CRediT authorship contribution statement

Eissa Fathalla: Writing – original draft, Visualization, Validation, Methodology, Investigation, Data curation, Conceptualization. **Boyan Mihaylov:** Writing – review & editing, Supervision, Resources, Project administration, Funding acquisition, Conceptualization.

Declaration of Competing Interest

The authors have no conflicts of interest to disclose.

Acknowledgement

The project was funded by the Service Public de Wallonie, Belgium, under Belgian Wallonia Research (BEWARE) fellowships according to agreement number 2010240. Moreover, the authors would like to express their gratitude to CLOQUETTE (Belgium) for providing the high strength concrete, and BEKAERT (Belgium) for providing the steel fibers, which were used for casting the high-strength fiber reinforced concrete (HFRC) jackets.

Data Availability

Data will be made available on request.

References

[1] Tan KH, Tjandra RA. Strengthening of RC continuous beams by external prestressing. J Struct Eng 2007;133(2):195–204.
[2] El-Shafiey T, Atta A. Retrofitting of reinforced concrete beams in shear using external prestressing technique. Mag Concr Res 2012;64(3):201–11.
[3] Macdonald MD, Calder AJJ. Bonded steel plating for strengthening concrete structures. Int J Adhes Adhes 1982;2(2):119–27.
[4] Adhikary BB, Mutsuyoshi H, Sano M. Shear strengthening of reinforced concrete beams using steel plates bonded on beam web: experiments and analysis. Constr Build Mater 2000;14(5):237–44.
[5] Lee HK, Cheong SH, Ha SK, Lee CG. Behavior and performance of RC T-section deep beams externally strengthened in shear with CFRP sheets. Compos Struct 2011;93(2):911–22.
[6] Kumari A, Patel SS, Nayak AN. Shear strengthening of RC deep beam using externally bonded GFRP fabrics. J Inst Eng (India) 2018;99:341–50 (Series A).
[7] Wang YD, Yang S, Han M, Yang X. Experimental study of section enlargement with reinforced concrete to increase shear capacity for damaged reinforced concrete beams. Appl Mech Mater 2013;256:1148–53.
[8] Buyukozturk O, Gunes O, Karaca E. Progress on understanding debonding problems in reinforced concrete and steel members strengthened using FRP composites. Constr Build Mater 2004;18(1):9–19.
[9] Li J, Gong J, Wang L. Seismic behavior of corrosion-damaged reinforced concrete columns strengthened using combined carbon fiber-reinforced polymer and steel jacket. Constr Build Mater 2009;23(7):2653–63.
[10] Thermou GE, Pantazopoulou SJ, Elnashai AS. Global interventions for seismic upgrading of substandard RC buildings. J Struct Eng 2012;138(3):387–401.
[11] Zollo RF. Fiber-reinforced concrete: an overview after 30 years of development. Cem Concr Compos 1997;19(2):107–22.
[12] Chasioti SG, Vecchio FJ. Shear behavior and crack control characteristics of hybrid steel fiber-reinforced concrete panels. Acids Struct J 2017;114(1):209.
[13] Tiberti G, Trabucchi I, AlHamaydeh M, Minelli F, Plizzari G. Crack control in concrete members reinforced by conventional rebars and steel fibers. IOP Conf Ser: Mater Sci Eng 2017;246(1)):012008.
[14] Bischoff PH. Tension stiffening and cracking of steel fiber-reinforced concrete. J Mater Civ Eng 2003;15(2):174–82.
[15] Ahmad W, Alabduljabbar H, Deifalla AF. An overview of the research trends on fiber-reinforced shotcrete for construction applications. Rev Adv Mater Sci 2023;62 (1):20230144.
[16] Islam MR, Mansur MA, Maalej M. Shear strengthening of RC deep beams using externally bonded FRP systems. Cem Concr Compos 2005;27(3):413–20.
[17] Li W, Leung CK. Shear span–depth ratio effect on behavior of RC beam shear strengthened with full-wrapping FRP strip. J Compos Constr 2016;20(3): 04015067.
[18] Rasheed MM. Retrofit of reinforced concrete deep beams with different shear reinforcement by using CFRP. Civ Environ Res 2016;8(5).
[19] Zhang Z. Shear Strengthening of RC Beams Using Carbon Fiber Reinforced Polymer Laminates. PhD Dissertation, New Jersey Institute of Technology,; 2003.
[20] Fathalla E, Rajapakse RMCM, Mihaylov BI. Modeling the shear behavior of deep beams strengthened with FRP sheets. Eng Struct 2022;260:114232.
[21] Ruano G, Isla F, Pedraza RI, Sfer D, Luccioni B. Shear retrofitting of reinforced concrete beams with steel fiber reinforced concrete. Constr Build Mater 2014;54: 646–58.
[22] Li R, Deng M, Zhang Y, Wei D. Shear strengthening of reinforced concrete deep beams with highly ductile fiber-reinforced concrete jacket. J Build Eng 2022;48: 103957.
[23] Mihaylov BI, Bentz EC, Collins MP. Two-parameter kinematic theory for shear behavior of deep beams. Acids Struct J 2013;110(3).
[24] Mihaylov B. Five-spring model for complete shear behaviour of deep beams. Struct Concr 2015;16(1):71–83.
[25] (⟨https://cloquette.be/products/groutex-profil-1/⟩) Accessed: 29th April 2024.
[26] (⟨https://www.bekaert.com/en/product-catalog/content/dop/dramix-ol-ce-documents⟩). Accessed: 29th April 2024.
[27] AFNOR, 2016. NF P18–470- Bétons fibrés à Ultra Hautes Performances-Spécifications, performance, production et conformité.
[28] Correlated Solutions. VIC-3D photo processing software [online]. Irmo, South Carolina: Correlated Solutions Inc. 2023. Available from: ⟨https://www.correlatedsolutions.com/vic-3d⟩.
[29] Trandafir AN, Palipana DK, Proestos GT, Mihaylov BI. Framework for crack-based assessment of existing lightly reinforced concrete deep members. Acids Struct J 2022;119(1):255–66.